Intranephronic Calculosis in Rats

An Ultrastructural Study

Hai T. Nguyen, VMD, MS, and J. Carroll Woodard, DVM, PhD

Female Sprague-Dawley rats weighing 45-55 g fed a purified diet for 18 days developed hydroxyapatite intratubular lithiasis, the earliest calcific lesions being detectable by light microscopy on Day 12. The kidneys from these rats revealed ultrastructural changes in proximal tubular cells prior to intraluminal microlith formation. These changes included evidence for increased intracellular calcium, accumulation of electron-dense cytoplasmic granules, and vesiculation and shedding of brush border microvilli within Segment I of the proximal tubule. It was concluded, on the basis of ultrastructural observation, that microvesicles were formed by the shedding of vesiculated microvilli and microvesicles initiated the formation of an intraluminal microurolith in Segment I of the proximal tubule. The initially formed microurolith grew, as it traveled down the nephron, to a size large enough to be visualized by light microscopy. When it reached Segment III (straight segment) of the proximal tubule, the microurolith reached a size so large that it became difficult for it to pass the loop of Henle. (Am J Pathol 1980, 100:39-56)

SPONTANEOUS INTRANEPHRONIC CALCULOSIS, or nephrocalcinosis, as it is commonly called, in the laboratory rat fed various purified diets has been reported by many investigators.[1-13] These diets usually contain levels of protein, vitamins, and minerals equal to or in slight excess of those recommended by the National Research Council (NRC).[14] Many of the commonly used strains of rats were affected by this condition. There seems to be some strain difference, but the degree and incidence of nephrocalcinosis has been consistently observed to be greater in the female rat.[2-13] Characteristically, the renal lesions were found at the corticomedullary junction and consisted of mineral deposition mainly in the lumens of proximal tubules. These mineral deposits appeared to contain calcium, phosphorus, and a glycoprotein matrix. Calcification was not observed in other organs, and chemical changes in the blood and urine of the affected animals were minimal.[8] This condition has also been observed in rats fed a commercially prepared pelleted diet as well.[5]

In a preliminary study by the authors, the AIN-76 purified diet for rats and mice [15] has been found to cause nephrocalcinosis consistently in female Sprague–Dawley rats. The animals fed a natural product laboratory

---

From the Division of Comparative Pathology, College of Veterinary Medicine, University of Florida, Gainesville, Florida.

Published as Florida Agricultural Experimental Stations Journal Series Number 2234.

Accepted for publication February 1, 1980.

Address reprint requests to J. Carroll Woodard, Box J-145, JHMHC, University of Florida, Gainesville, FL 32610.

0002-9440/80/0709-0039$01.00

rat diet (Rodent Lab Chow 500, by Ralston Purina Company, St. Louis, Mo) for the same period of time did not develop nephrocalcinosis.

The cause of nephrocalcinosis in the rat has been studied by many researchers. Urinary factors, estrogenic hormones, and various dietary components, including protein, lipid, and minerals, have all been studied and implicated. The exact etiologic conditions, however, remain unknown.

Experiments were conducted to investigate pathogenic mechanisms of renal calcification induced in rats by feeding a purified diet. Feeding times were adjusted to permit sequential ultrastructural observations before and during the development of hydroxyapatite microliths within the renal proximal tubule.

Materials and Methods

Female Sprague–Dawley rats (Charles River, Wilmington, Mass) weighing 45–55 g were used. Five groups consisting of 3 experimental and 2 control animals were fed AIN-76 diet or a control diet (Rodent Lab Chow 500) and were killed after 10, 12, 14, 16, and 18 days of feeding. These times were chosen on the basis of the findings of a preliminary study that the earliest histologically detectable calcified lesions in the kidneys appeared after 14 days of feeding the purified diet. The kidneys were perfused retrograde through the abdominal aorta as described by Maunsbach [16] and Griffith et al.[17] The perfusate contained 2.5% glutaraldehyde and 2% paraformaldehyde in 0.1 M cacodylate buffer, pH 7.2. Radiographs were taken of thin slices of the perfused kidneys in order to detect the presence of mineralization. For standard electron-microscopic examination, the tissue was washed for 30 minutes in cacodylate buffer, postfixed in 1% OsO_4 in the same buffer for 1 hour, dehydrated in a graded ethanol series, and embedded in Epon–araldite. Thick sections (0.5–1.0 μ) were stained with toluidine blue for light microscopy. Thin sections were stained with saturated aqueous uranyl acetate followed by Reynold's lead citrate [18] and examined with a Hitachi HU-11B or a Hitachi HU-11E electron microscope. Because mineral deposition in the tissues led to fragmentation of thin sections, sections were cut slightly thicker than standard in order to preserve anatomical relationships. Potassium pyroantimonate was used to localize ionic calcium in the tissue at the ultrastructural level; the procedure was based on the methods described by Spicer et al [19] and Debras et al.[20] Alkaline phosphatase was visualized by the methods described by Tranzer [21] and Mayahara et al [22] and modified by Lewis.[23] The periodic-acid–silver-methenamine (PASM) staining technique was used to detect the presence of carbohydrates; the method was that described by Rambourg [24] and Martino and Zamboni.[25] Pronase digestion was performed according to the procedure described by Anderson and Andre.[26] Microprobe X-ray analysis was carried out with an energy-dispersive X-ray microanalysis system having a Kevex X-ray detector and a Kevex Micro X-ray Computer Analyzer Model 7000 attached to a JEOL 100CX electron microscope.

Results

No renal calcification was observed in rats fed the AIN-76 diet and killed on Day 10. At Day 12, 1 out of 3 animals showed slight calcification, which was barely detected radiographically (Figure 1). At Days 14 and 16, 2 of 3 animals showed slight calcification, and at Day 18 all animals had renal calcification ranging from slight to severe. All animals fed the control diet were free of renal calcification.

The earliest renal ultrastructural changes in rats killed on Day 10 were vesiculation of proximal tubular microvilli (Figures 3 and 4) and the appearance of electron-dense granules in the cytoplasm as well as in large vacuoles near the brush border (Figure 2). An increase in the number and size of intracytoplasmic vacuoles in the proximal tubules was apparent and was observed especially in the first segment. Electron-dense deposits within vacuoles were visualized in sections stained with uranyl acetate and lead citrate as well as in sections stained with potassium pyroantimonate. In addition to dense deposits, potassium pyroantimonate revealed an increased number of fine granules within the many vacuoles. The fine deposits seen in these vacuoles are presumably pyroantimonate–calcium complexes. These changes were also observed frequently in rats killed on Days 12, 14, 16, and 18, and the incidence increased with increasing frequency and severity of renal calcification. Sometimes large blebs containing electron-dense material were seen related to the microvillous surface of proximal tubular cells. These were thought to develop from vesiculated microvilli (Figures 5 and 6). Following potassium pyroantimonate staining, accumulation of electron-dense material was also found in intracytoplasmic vacuoles, within the interdigital spaces, the spaces between the plasma and basement membranes, and the endothelial cells lining blood vessels. A similar reaction was not found in sections from control animals.

Starting at Day 12, aggregates of cellular components were frequently found in proximal tubular lumens. These aggregates consisted mainly of fragments of brush border microvilli, vesiculated microvilli, and electron-dense bodies (Figure 7). Electron-dense material was seen deposited on these membranous aggregates in concentric layers, forming early microuroliths (Figures 8–10). These early laminated microuroliths were found mainly in the third, or last, segment of proximal tubules and most frequently in rats killed on Day 14. Cellular components, vesicles, and fragments of microvilli appeared to be a major component and were found in all layers of these early microuroliths (Figures 10–12). Occasionally microuroliths were found trapped in the brush border,[13] but most frequently they were seen free in the proximal tubular lumen (Figure 14). Some microuroliths appeared very dense (Figure 14). Only the cellular material attached to the surface of the urolith could be recognized, but the laminated configuration was still evident. This form of "mature" microurolith was found more frequently in rats killed on Days 16 and 18.

Other forms of mineral deposits were observed in the proximal tubules. Spherical aggregates of electron-dense granules were seen free in the proximal tubular lumens. These aggregates were not surrounded by membranes. They did not have a laminated structure and did not contain cellu-

lar components. Nonlaminated microuroliths were dense and contained needle-shaped crystals characteristic of hydroxyapatite (Figure 15). This is best seen at the periphery of the microurolith. The nonlaminated form was less frequently seen than the laminated form and was only found in rats killed at later times (Days 16 and 18).

Extensive lesions and tubular necrosis were only observed in the presence of severe renal calcification (mainly by Day 18), which sometimes also involved the loops of Henle as well as the distal tubules.

Alkaline phosphatase activity in the proximal and distal tubules appeared to be increased in rats killed on Day 14, compared with control rats. No changes in alkaline phosphatase activity were observed at other times.

The results of X-ray microanalysis indicate that the crystals are made of calcium and phosphate salts. The only notable peaks seen in the X-ray energy spectrum from the crystal were those of calcium and phosphorus. Results of mapping for Ca and P of the same crystal further confirmed that Ca and P were the main components of the crystals.

Discussion

Prior to calcification, significant renal ultrastructural changes were observed only in cells of Segment I of proximal tubules. These changes include vesiculation of the brush border microvilli, increase in number and size of intracytoplasmic vacuoles, and accumulation of electron-dense granules, which were reactive to potassium pyroantimonate. Potassium pyroantimonate also gave evidence of an increase in intracellular ionic Ca prior to calcification. Potassium pyroantimonate can form precipitates with sodium, calcium, and magnesium and is a useful tool for examining the subcellular distribution of these inorganic cations. The specificity of potassium pyroantimonate for calcium under the reaction conditions used in this experiment has been discussed.[19,20] We removed sodium from the tissue by washing the tissue with distilled water. We further verified the specificity of the stain by having selected tissue samples treated with EGTA before pyroantimonate staining. In addition, X-ray microanalysis failed to indicate the presence of magnesium within intraluminal microliths.

Electron-dense calcium precipitates were seen in vesiculated microvilli that appeared to fragment from the cell surfaces. The formation of hernialike evaginations of the apical cytoplasm has been described in hypervitaminosis-D–induced nephrocalcinosis,[27] and the release of large granules of calcium precipitates into the lumen was thought to occur in renal calcification induced by parathormone.[28] Extracellular matrix vesicles are

believed to induce calcification in epiphyseal cartilage by nucleating calcium phosphate precipitation.[29,30] Radiotracer studies of lipid synthesis and transport in cartilage lead to the conclusion that matrix vesicles in the growth plate are derived from chondrocytes, probably by budding from cellular processes.[30] Vesicles, morphologically similar to matrix vesicles, have also been described in calcification of human aortic valve and aortic media.[31] It is possible that the mechanism of the intraluminal apatite formation in rats fed the AIN-76 diet is initiated by a process that causes vesiculation of microvilli and release of calcium-rich membranous processes (microvesicles) into the lumen of Segment I of the proximal tubule.

Following the intracellular changes, cellular components appear in the proximal tubular lumen in large quantities. Since they were PASM-reactive, these cellular components were considered to represent tips of proximal tubular microvilli and vesicles probably of microvillous origin (Figure 11). Mineralization occurred in concentric layers, and cellular components became organized into laminated, spherical structures. A microcalculus formed measuring 3–5 μ in diameter. The tips of brush border microvilli were observed to be shed into the tubular lumen, and these appeared to be active not only in the initial organic nidus formation but also in the subsequent laminar growth of the crystal. It has been suggested that matrix formation preceded crystal formation in all forms of experimental intranephronic calculosis, and mineralization in terms of inorganic accretion by matrix has been suggested as a distinct possibility by Boyce.[32]

In the second type of intraluminal microlith, observed somewhat later in the course of the experiment, an organized internal structure could not be visualized. These crystals had a spherical shape and an amorphous appearance. It is possible that these crystals may have evolved from aggregates of distinct electron-dense granules observed earlier in the proximal tubular lumen by gradually accumulating apatite crystals until the internal structure became obscure. Amorphous, unorganized calcium deposits are commonly seen in damaged or necrotic tissues. The nonlaminated, amorphous microcrystals described here were seen free in the proximal tubular lumens. There was no evidence of extensive cellular injury or necrosis in nephrons proximal to the location where the microcalculus was found. Even in advanced cases (Day 18), tubular lesions such as sloughing of brush border or cellular necrosis appeared to be related to mechanical insult by the microlith rather than to be a cause of calcification. Vermeulen and Lyon have shown that calculus formation can occur *in vitro* without involvement of an organic matrix.[33] It is also implied from this work that microliths in the kidney can be formed by aggregation of particles that are freely moving along the renal tubule. In recent years there has

been a resurgence of interest in the physicochemical features of urolithiasis, and much interest has been shifted from the role of organic matrix to that of one salt's inducing by epitaxy the precipitation of another salt. The role of inhibitors affecting crystal formation and aggregation has also received increasing attention.[34,35] The role of organic matrix in renal calculus formation has not been shown before. The demonstration of vesiculation and shedding of proximal tubule microvilli and later formation of laminated microlith containing vesicles of microvillous origin supports the role of organic matrix in renal microlith formation. Microliths were observed in which matrix vesicles were not visualized. However, this form of nonlaminated microlith was only observed later in the course of the experiment (Days 16 and 18) and could have resulted from the accretion of small microvillar fragments or been so highly mineralized that the matrix could not be visualized.

The results of X-ray microanalysis and mapping indicate that the crystals contained Ca and P. This finding is in agreement with the X-ray diffraction results of Woodard [8] and Cousins and Geary,[5] who showed the mineral was hydroxyapatite. Intranephronic calculosis, induced by the AIN-76 diet, bears certain ultrastructural characteristics that distinguish it from other forms of renal calcification experimentally induced by chloride depletion, Mg deficiency, Ca and vitamin D toxicity, and parathormone and phosphate administration. In chloride depletion, calcific deposits were formed in lysosome-like bodies and mitochondria.[36] Renal calcification induced by large doses of Ca or vitamin D is characterized by extensive cellular degeneration and necrosis and widespread calcified lesions with involvement of basement membrane and mitochondria.[37-39] Large doses of phosphate also cause severe tubular necrosis and widespread calcification, the medulla being the most severely affected part.[40] Calcification of mitochondria and basement membrane and severe renal lesions were not observed in tubular lithiasis experimentally induced by the feeding of the AIN-76 diet and similar purified diets. In Mg deficiency there is edema of proximal tubular epithelium, and calcification is also seen in the loops of Henle, collecting tubules, and other organs such as the heart, and skeletal muscle.[41,42] Early renal calcification induced in this experiment was restricted to the proximal tubules.

Unpublished data by the authors have implicated the dietary level of phosphorus as being a major factor causing renal calcification when female rats are fed the AIN-76 diet. Results from studies of the composition of glomerular filtrate in rats by micropuncture [43] have shown that the resorption of phosphate in proximal tubules is less avid in the female than in the male. Micropuncture studies of renal adaptation to the supply and re-

quirement of phosphate in rats have shown evidence of a special adaptive mechanism for regulating inorganic phosphate in the renal tubule in response to the rat's bodily need.[44] This adaptive mechanism, which is parathyroid-independent, selectively modifies the sodium-dependent phosphate uptake by brush border membrane vesicles by altering the phosphate transport system bound to the luminal membrane of the proximal tubule.

Calcium is known to be resorbed by the proximal tubule. There is no evidence for calcium secretion by the tubules, although transtubular flux of calcium has been observed.[45] Therefore, if the increased number and size of intracytoplasmic vacuoles within the cytoplasm and the accumulation of electron-dense granules that were potassium–pyroantimonate–reactive are part of an active process, they probably represent increased calcium resorption. One mechanism involves the tubular reabsorption of phosphate's being dependent upon the proximal tubular transport of calcium and/or on the accumulation of intracellular calcium phosphate. Thus, when calcium transport by the proximal tubular cells is high, the reabsorption of phosphate is depressed, and there is a phosphaturia that tends to lower the level of plasma phosphate. The increased number of electron-dense granules within Segment I of the proximal tubular prior to urolithiasis lends morphologic support to this mechanism. In addition, there is morphologic evidence that suggests that exaggeration of this process may lead to vesiculation and shedding of microvilli that contain calcium. The microvesicles thus formed are important in the initiation and growth of microuroliths within the lumen of the proximal tubule.

References

1. Forbes RM: Mineral utilization in the rat. I. Effects of varying dietary ratios of calcium, magnesium, and phosphorus. J Nutr 1963, 80:321–326
2. Cousins FB, Geary CPM: A sex-determined renal calcification in rats. Nature 1966, 211:980–981
3. Goulding A, Malthus RS: Effect of dietary magnesium on the development of nephrocalcinosis in rats. J Nutr 1969, 97:353–358
4. De Groot AP, Slump P: Effects of severe alkali treatment of proteins on amino acid composition and nutritive value. J Nutr 1969, 45–56
5. Geary CP, Cousins FB: An oestrogen-linked nephrocalcinosis in rats. Br J Exp Pathol 1969, 50:507–515
6. Woodard JC: On the pathogenesis of alpha protein–induced nephrocytomegalia. Lab Invest 1969, 20:9–16
7. Du Bruyn DB: A comparison of certain rat strains with respect to susceptibility to nephrocalcinosis. S Afr Med J 1970, 44:1417–1418
8. Woodard JC: A morphologic and biochemical study of nutritional nephrocalcinosis in female rats fed semi-purified diets. Am J Pathol 1971, 65:253–268
9. Woodard JC: Relationship between the ingredients of semi-purified diets and nutritional nephrocalcinosis of rats. Am J Pathol 1971, 65:269–278

10. Du Bruyn DB: Nephrocalcinosis in the white rat. S Afr Med J 1972, 46:1588–1593
11. Van Beek L, Feron VJ and De Groot AP: Nutritional effects of alkali-treated soy protein in rats. J Nutr 1974, 104:1630–1636
12. Kaunitz H, Johnson RE: Dietary protein, fat and minerals in nephrocalcinosis in female rats. Metabolism 25:69-77, 1976
13. Struthers BJ, Dahlgren RR, Hopkins DT: Biological effects of feeding graded levels of alkali-treated soybean protein containing lysinoalanine (N^E-2 [carboxyethyl] L-lysine) in Sprague–Dawley and Wistar rats. J Nutr 1977, 107:1190–1199
14. National Research Council: Nutrient Requirements of Laboratory Animals. No. 10. 3rd revised edition. National Academy of Sciences, Washington, DC, 1978
15. American Institute of Nutrition: Report of the American Institute of Nutrition Ad Hoc Committee on Standards for Nutritional Studies. J Nutr 1977, 107:1340–1348
16. Maunsbach AB: The influence of different fixatives and fixation methods on the ultrastructure of rat kidney proximal tubule cells. J Ulstruct Res 1966, 15:242–282
17. Griffith LD, Bulger RE, Trump BF: The ultrastructure of the functioning kidney. Lab Invest 1967, 16:220–246
18. Reynolds ES: The use of lead citrate at high pH as an electron opaque stain in electron microscopy. J Cell Biol 1963, 17:208–212
19. Spicer SS, Hardin JH, Greene WB: Nuclear precipitates in pyroantimonate-osmium tetroxide-fixed tissues. J Cell Biol 1968, 39:216–221
20. Debras G, Hoffman L, Landon EJ, Hurwitz L: Electron microscopic localization of calcium in vascular smooth muscle. Anat Rec 1975, 182:447–472
21. Tranzer JP: Utilisation de citrate de plomb pour la mise en évidence de la phosphatase alcaline au microscope électronique. J Microscopie 1965, 4:409–412
22. Mayahara H, Hirano H, Saito T, Ogawa K: The new lead citrate method for the ultracytochemical demonstration of activity of non-specific alkaline phosphatase (orthophosphoric monoester phosphohydrolase). Histochemie 1967, 88–96
23. Lewis PR: Metal precipitation methods for hydrolytic enzymes, Staining Methods for Sectioned Material. Edited by AM Glauert. New York, North-Holland Publishing Company, 1977, 137–223
24. Rambourg A: An improved silver methenamine technique for the detection of periodic acid–reactive complex carbohydrates with the electron microscope. J Histochem Cytochem 1967, 15:409–412
25. Martino CD, Zamboni L: Silver methenamine stain for electron microscopy. J Ultrastruct Res 1967, 272–282
26. Anderson WA, André J: The extraction of some cell components with pronase and pepsin from thin sections of tissue embedded in an epon–araldite mixture. J Microsc 1968, 7:343–354
27. Blagodarov VN: [Kidney ultrastructre in experimental nephrolithiasis and nephrocalcinosis]. Biull Eksp Biol Med 1976, 81:494–496
28. Engfeldt B, Gardell S, Hellstrom J, Ivemark B, Rhodin J, Strandh J: Effect of experimentally induced hyperparathyroidism on renal function and structure. Acta Endocrinol (Copenh) 1958, 29:15–26
29. Felix R, Fleisch H: Role of matrix vesicles in calcification. Fed Proc 1976, 35:169–171
30. Rabinovitch AL, Anderson HC: Biogenesis of matrix vesicles in cartilage growth plates. Fed Proc 1976, 35:112–116
31. Kim KM: Calcification of matrix vesicles in human aortic valve and aortic media. Fed Proc 1976, 35:156–162
32. Boyce WH: Organic matrix of human urinary concretions. Am J Med 1968, 45:673–683
33. Vermeulen CW, Lyon ES: Mechanisms of genesis and growth of calculi. Am J Med 1968, 145:684–692

34. Finlayson B: Physicochemical aspects of urolithiasis. Kidney Int 1978, 13:344–360
35. Fleisch H: Inhibitors and promoters of stone formation. Kidney Int 1978, 13:361–371
36. Sarkar K, Tolnai G, Levine DZ: Nephrocalcinosis in chloride depleted rats: An ultrastructural study. Calc Tiss Res 1973, 12:2–7
37. Duffy JL, Yasunosuke S, Chung J: Acute calcium nephropathy: Early proximal tubular changes in the rat kidney. Arch Pathol 1971, 91:340–350
38. Ganote CE, Philipsborn DS, Chen E, Carone FA: Acute calcium nephrotoxicity. Arch Pathol 1975, 99:650–657
39. Scarpelli DG: Experimental nephrocalcinosis: A biochemical and morphologic study. Lab Invest 1965, 114:123–141
40. Craig JM: Observations on the kidney after phosphate loading in the rat. Arch Pathol 1959, 68:306–315
41. Schneeberger EE, Morrison AB: The nephropathy of experimental magnesium deficiency. Lab Invest 1965, 14:674–686
42. Heroux O, Peter D, Heggtveit A: Long-term effect of suboptimal dietary magnesium on magnesium and calcium contents of organs, on cold tolerance and on lifespan, and its pathological consequences in rats. J Nutr 1977, 107:1640–1652
43. Harris CA, Baer PG, Chirito E, Dirks JH: Composition of mammalian glomerular filtrate. Am J Physiol 1974, 227:972–976
44. Bonjour JP, Muhlbauer RC, Caverzasio J, Fleisch H: Renal adaptation to the supply and requirement of phosphate. Calc Tiss Int 1979, 27 (Suppl): A3
45. Bronner F, Thompson DD: Renal transtubular flux of electrolytes in dogs with special reference to calcium. J Physiol 1961, 157:232–250

[*Illustrations follow*]

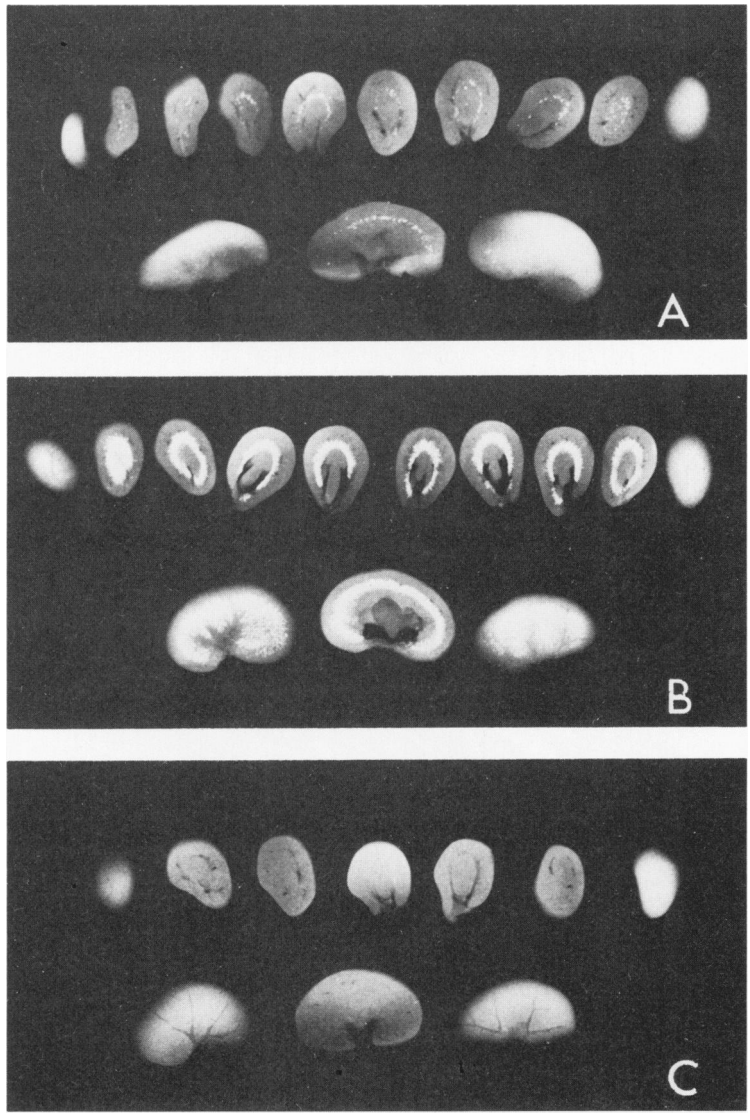

Figure 1—Radiographs of 1-mm thick transverse and longitudinal sections of rat kidneys showing **(A)** slight calcification, **(B)** severe calcification, and **(C)** negative control.

2

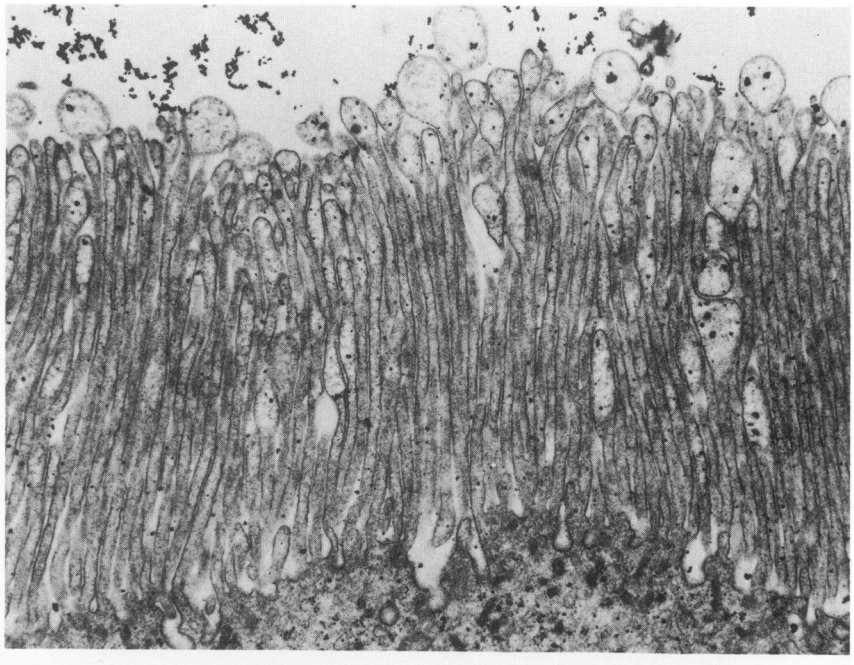

3

Figures 2 and 3—Proximal tubules of a rat killed on Day 10. Note the vesiculation of proximal tubular microvilli. (×20,000)

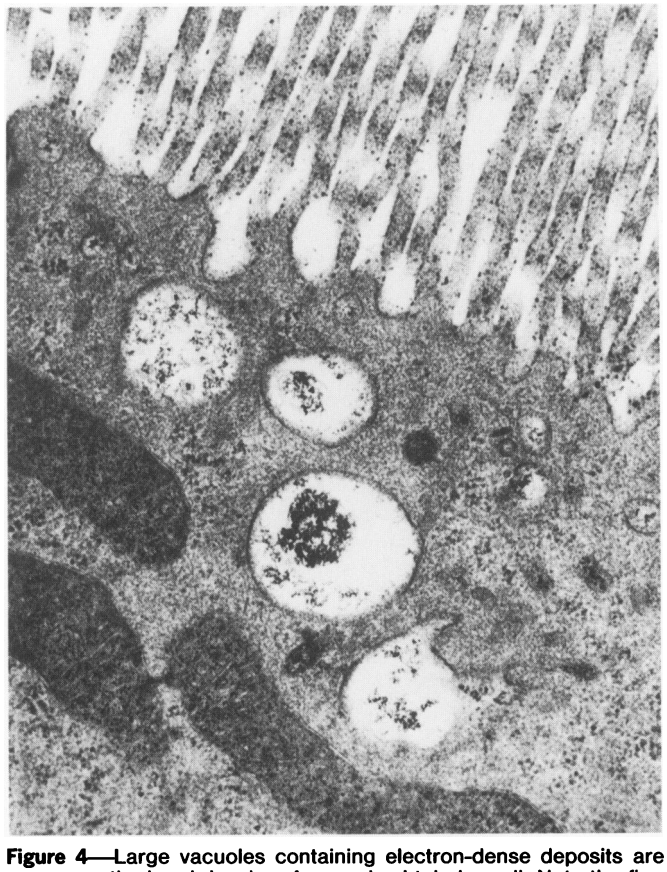

Figure 4—Large vacuoles containing electron-dense deposits are seen near the brush border of a proximal tubular cell. Note the fine granules of Ca–pyroantimonate complex on the brush border microvilli. (Potassium pyroantimonate stain, ×40,000)

5

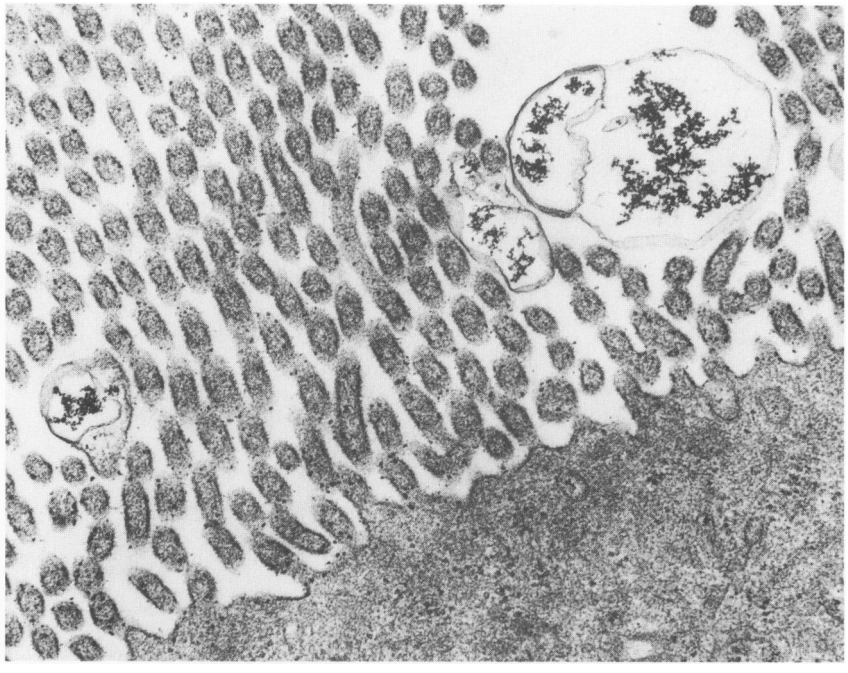

6

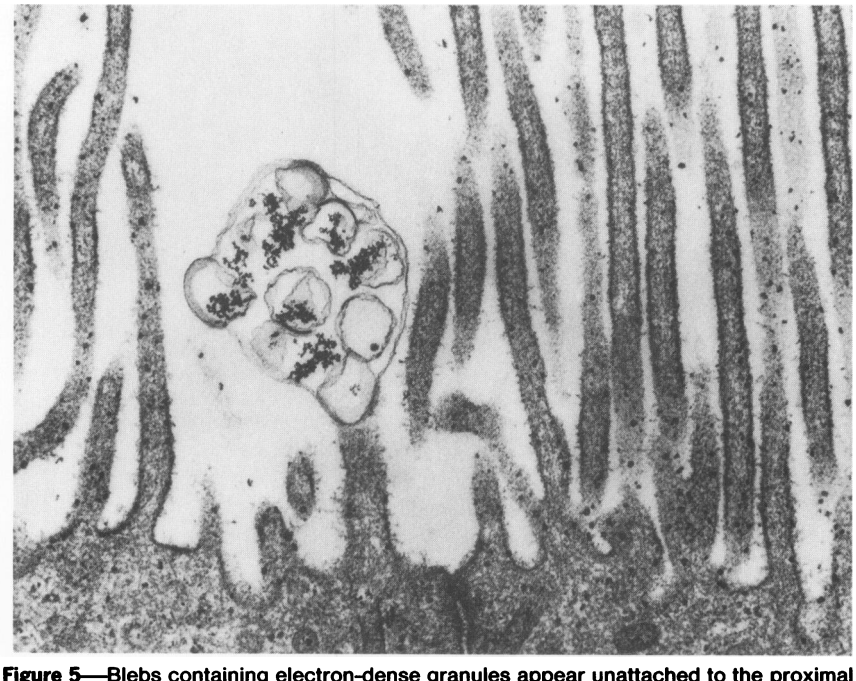

Figure 5—Blebs containing electron-dense granules appear unattached to the proximal tubular cell. (Potassium pyroantimonate stain, ×40,000) **Figure 6**—Proximal tubular cell shows an aggregate of several small blebs with electron-dense granules. (Potassium pyroantimonate stain, ×55,000)

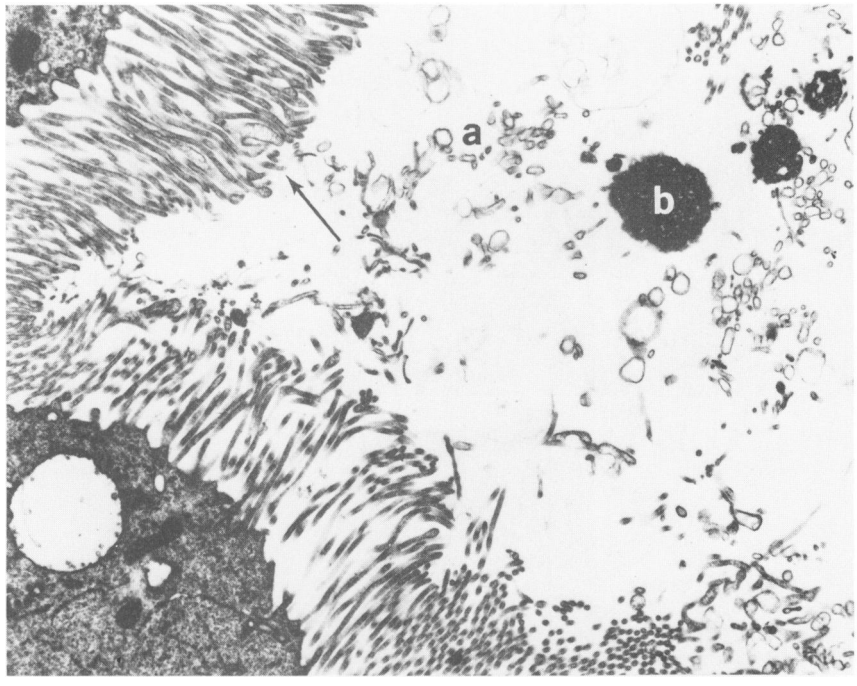

7

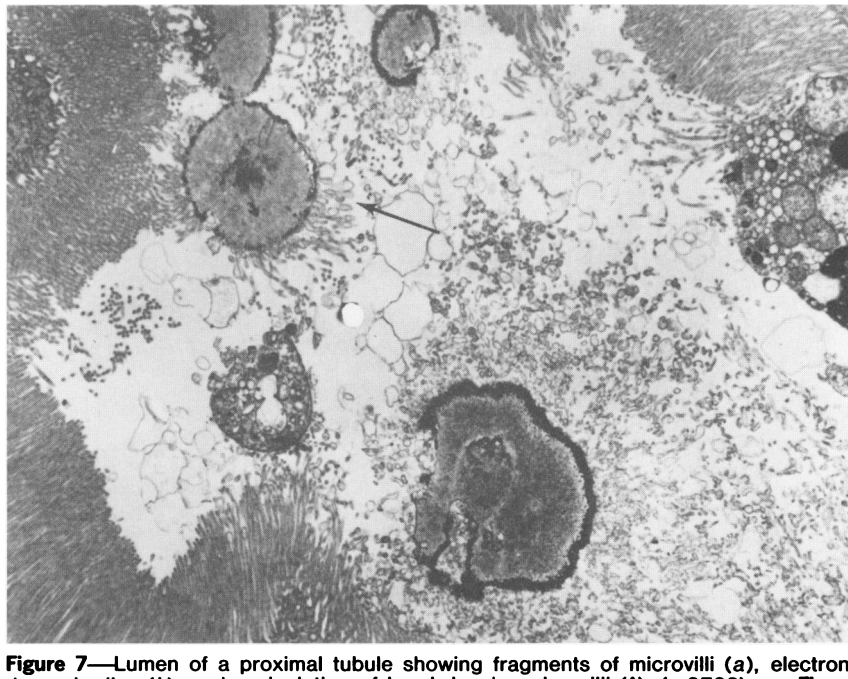

8

Figure 7—Lumen of a proximal tubule showing fragments of microvilli (*a*), electron-dense bodies (*b*), and vesiculation of brush border microvilli (↑). (×9700) **Figure 8**—Lumen of a proximal tubule containing four microliths. Note the elecron-dense material at the center of some microliths and at the periphery of all microliths. Fragments of swollen microvilli adhere peripherally (↑). ×11,200)

Figure 9—A small microlith with a distinct concentric, laminated configuration in the lumen of a proximal tubule at the junction of a loop of Henle. (×7000)

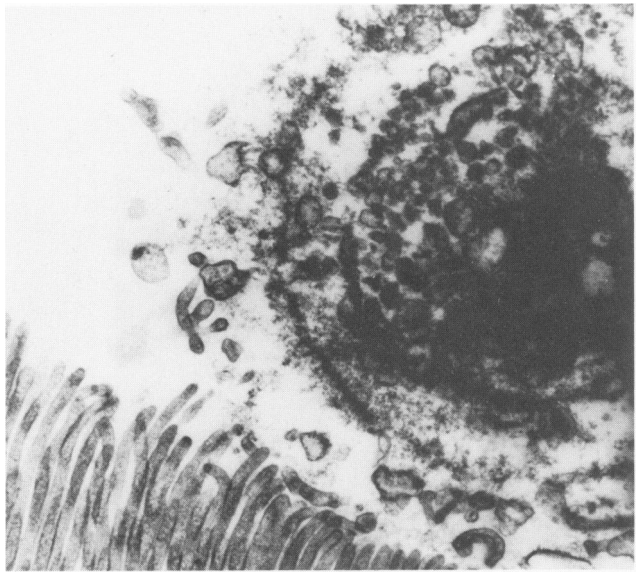

Figure 10—Higher magnification of microlith showing vesicles and cellular components in all concentric layers of the microlith. (×29,000)

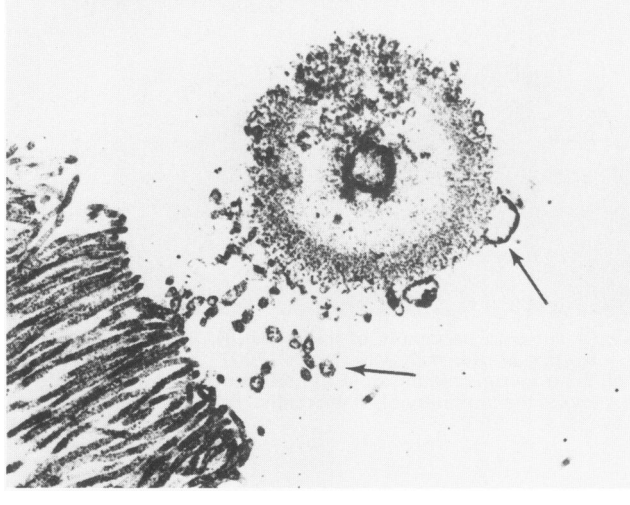

Figure 11—A small laminated microlith in a proximal tubule showing PA-silver-reactive material in all layers of the microlith. Vesicles and microvilli fragments also show PA-silver-reactive membrane (↑). (PASM stain, ×12,000)

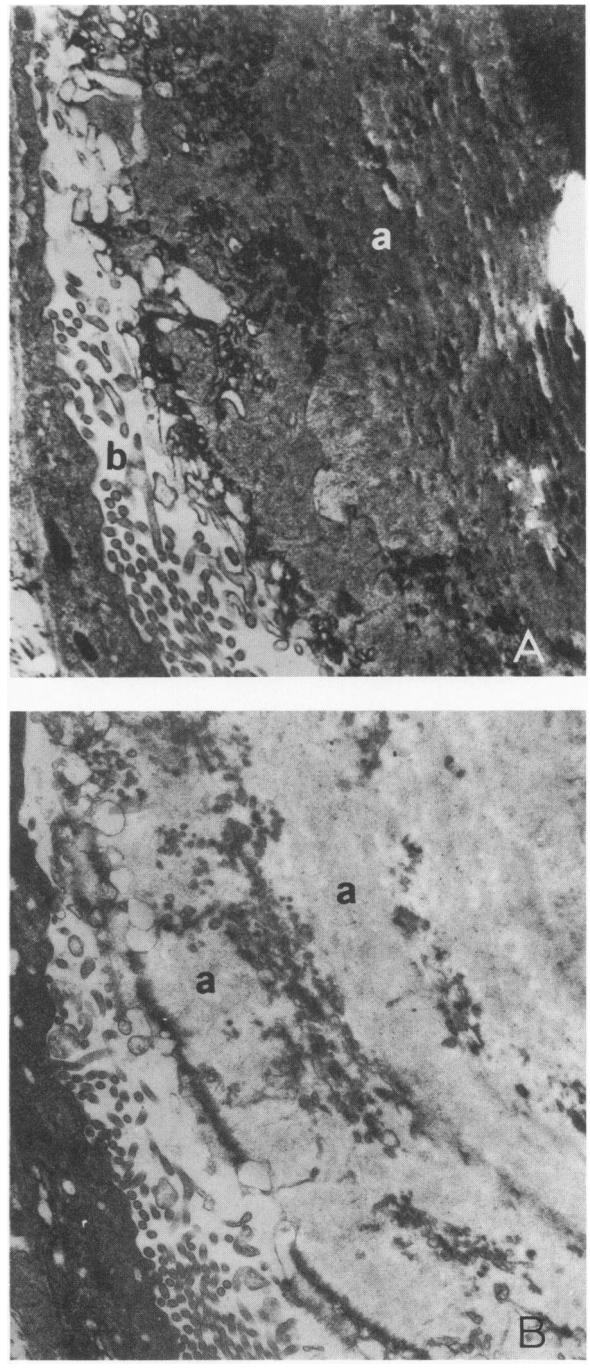

Figure 12—Pronase digestion of a laminated microlith in a proximal tubule. **A**—Control, portion of a microlith (*a*) in the lumen of proximal tubule with the brush border partially destroyed (*b*).

B—The same microlith after pronase digestion. The concentric layers (*a*) are less electron-dense than the corresponding areas in the control. (×18,000)

13

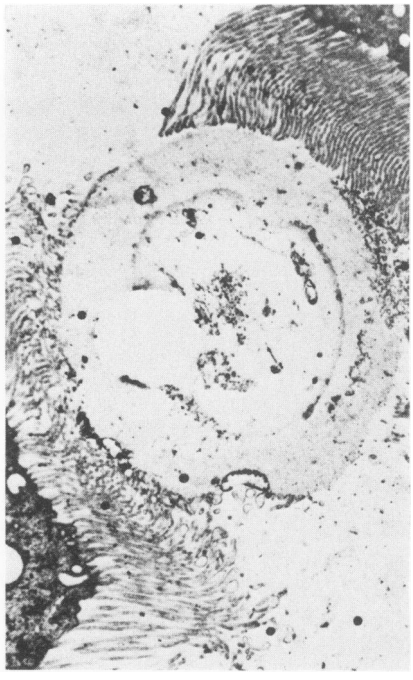

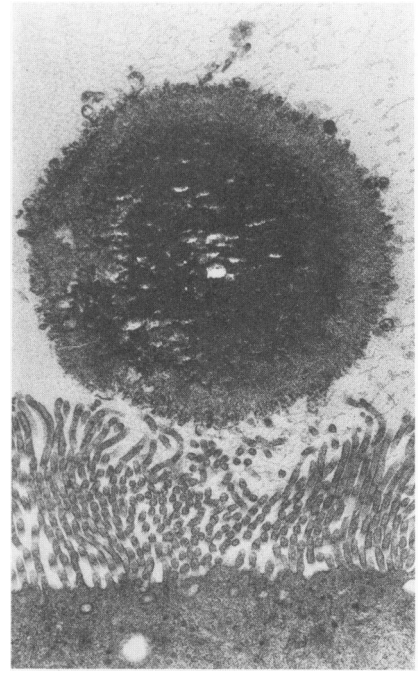

14

15

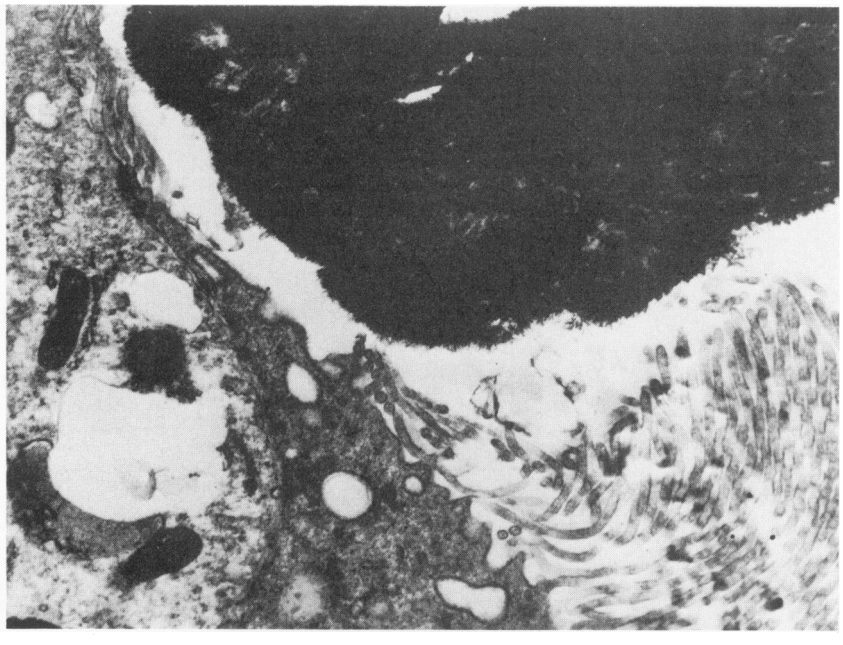

Figure 13—A laminated microlith is apparently trapped in the narrow lumen of a proximal tubule. (PASM stain, ×7900) **Figure 14**—A laminated and compact microlith free in the lumen of a proximal tubule. No cellular fragments are seen within the microlith. (×15,000) **Figure 15**—A nonlaminated, solid microlith in the lumen of a proximal tubule showing, at the periphery, the needle-shaped crystals characteristic of hydroxyapatite. (×24,000)